Mon. Not. R. Astron. Soc. **396,** 511–522 (2009) doi:10.1111/j.1365-2966.2009.14728.x

Signals of statistical anisotropy in *WMAP* foreground-cleaned maps

Pramoda Kumar Samal,[1⋆] Rajib Saha,[2,3⋆] Pankaj Jain[1⋆] and John P. Ralston[4⋆]

[1]*Department of Physics, Indian Institute of Technology, Kanpur, U.P. 208016, India*
[2]*Jet Propulsion Laboratory, M/S 169-327, 4800 Oak Grove Drive, Pasadena, CA 91109, USA*
[3]*California Institute of Technology, Pasadena, CA 91125, USA*
[4]*Department of Physics & Astronomy, University of Kansas, Lawrence, KS 66045, USA*

Accepted 2009 March 2. Received 2008 November 12

ABSTRACT

Recently, a symmetry-based method to test for statistical isotropy of the cosmic microwave background was developed. We apply the method to template-cleaned 3- and 5-years *Wilkinson Microwave Anisotropy Probe-Differencing Assembly* maps. We examine a wide range of angular multipoles from $2 < l < 300$. The analysis detects statistically significant signals of anisotropy inconsistent with an isotropic cosmic microwave background in some of the foreground-cleaned maps. We are unable to resolve whether the anomalies have a cosmological, local astrophysical or instrumental origin. Assuming the anisotropy arises due to residual foreground contamination, we estimate the residual foreground power in the maps. For the *W*-band maps, we also find a highly improbable degree of isotropy we cannot explain. We speculate that excess isotropy may be caused by faulty modelling of detector noise.

Key words: methods: data analysis – cosmic microwave background – cosmology: miscellaneous.

1 INTRODUCTION

The inflationary big bang model assumes that anisotropies of the cosmic microwave background (CMB) come from random isotropic perturbations in the early universe. However, there are indications that cosmological observables may not be isotropic. The indications include distributions of polarizations from radio galaxies (Birch 1982; Kendall & Young 1984; Jain & Ralston 1999; Jain & Sarala 2006), statistics of optical polarizations from quasars (Hutsemékers 1998; Hutsemékers & Lamy 2001; Jain, Narain & Sarala 2004) and many studies of unpolarized CMB data. The CMB studies indicate an alignment of the low-*l* multipoles (de Oliveira-Costa et al. 2004; Ralston & Jain 2004; Schwarz et al. 2004) and a hemispherical anisotropy (Eriksen et al. 2004). The indications of violation of isotropy in CMB data has prompted substantial activity with varying outcomes (Bielewicz, Górski & Banday 2004; Hansen, Banday & Górski 2004; Katz & Weeks 2004; Bielewicz et al. 2005; Prunet et al. 2005; Bernui et al. 2006; Copi et al. 2006; de Oliveira-Costa & Tegmark 2006; Freeman et al. 2006; Wiaux et al. 2006; Bernui et al. 2007; Copi et al. 2007; Eriksen et al. 2007b; Helling, Schupp & Tesileanu 2007; Land & Magueijo 2007; Magueijo & Sorkin 2007; Bernui 2008; Lew 2008). Differences arise due to different tests being used by different authors (Efstathiou 2003; Hajian, Souradeep & Cornish 2004; Donoghue & Donoghue 2005; Hajian & Souradeep 2006) and radio (Bietenholz & Kronberg 1984) in CMB data. Despite a measure of controversy, it is astonishing that diverse data sets all indicate a common axis of anisotropy, pointing roughly in the direction of the Virgo supercluster (Ralston & Jain 2004).

The possible violation of statistical isotropy in CMB has led to many theoretical studies (Cline, Crotty & Lesgourgues 2003; Contaldi et al. 2003; Kesden, Kamionkowski & Cooray 2003; Armendariz-Picon 2004; Berera et al. 2004; Gordon et al. 2005; Land & Magueijo 2005; Moffat 2005; Vale 2005; Abramo, Sodre & Wuensche 2006; Inoue & Silk 2006; Land & Magueijo 2006; Rakic, Rasanen & Schwarz 2006; Campanelli, Cea & Tedesco 2007; Koivisto & Mota 2008; Naselsky, Verkhodanov & Nielsen 2008; Boehmer & Mota 2008; Kahniashvili, Lavrelashvili & Ratra 2008; Rodrigues 2008). The generation and evolution of primordial perturbations in an anisotropic universe have also been studied (Armendariz-Picon 2006; Battye & Moss 2006; Koivisto & Mota 2006; Gumrukcuoglu, Contaldi & Peloso 2007; Pereira, Pitrou & Uzan 2007) along with the possibility of anisotropic inflation (Hunt & Sarkar 2004; Buniy, Berera & Kephart 2006; Donoghue, Dutta & Ross 2007; Kanno et al. 2008; Yokoyama & Soda 2008). The possibility that foreground contamination can lead to alignment has been investigated (Gaztanaga et al. 2003; Slosar & Seljak 2004). Alternatively, it has been suggested that systematic and statistical errors in the extracted CMB signal may lead to the observed anomalies (Liu & Li 2008). There have also been some theoretical studies of the optical alignment effect (Jain, Panda & Sarala 2002; Hutsemékers et al. 2008; Payez, Cudell & Hutsemékers 2008). It may be possible to explain the violation of isotropy in CMB and radio polarizations due to some local effect. However, the alignment of optical polarizations depends on redshift, and hence cannot be attributed to a local effect (Jain et al. 2002).

⋆E-mail: samal@iitk.ac.in (PKS); Rajib.Saha@jpl.nasa.gov (RS); pkjain@iitk.ac.in (PJ); ralston@ku.edu (JPR)

In a recent paper (Samal et al. 2008), we introduced a new method for testing isotropy of CMB data. The method is based on identifying invariant relations between different multipoles. For each multipole $l \geq 2$ we identify three rotationally invariant eigenvalues of the power matrix A_{ij}, defined by

$$A_{ij} = \frac{1}{l(l+1)} \sum_{m,m'} a^*_{lm} (J_i J_j)_{mm'} a_{lm'} , \quad (1)$$

where $J_i (i = 1, 2, 3)$ are the angular momentum operators in representation l. The sum of the eigenvalues is the usual power C_l. The remaining independent combinations of eigenvalues provide information about the isotropy of the sample.

In an infinite isotropic sample all the eigenvalues of the power matrix would be equal. Statistical anisotropies in CMB data will certainly lead to statistical fluctuations in the eigenvalues. We quantify the fluctuations by introducing the concept of power entropy. The eigenvectors of the matrix A_{ij} also contain additional information. Their orientation should be random in truly isotropic data. We define the 'principal' eigenvector as the one associated with the largest eigenvalue. We then study the alignment entropy, which tests for alignment among different eigenvectors.

In Samal et al. (2008), we studied the *Wilkinson Microwave Anisotropy Probe* (*WMAP*) Interior Linear Combination (ILC) data set and restricted our attention to the multipole region $l \leq 50$. In this paper, we study the individual foreground cleaned Differencing Assembly (DA) maps, $Q1$, $Q2$, $V1$, $V2$, $W1$, $W2$, $W3$ and $W4$, also prepared by the *WMAP* team. We also extend the scope of analysis to the range $2 \leq l \leq 300$. As far as we know, these are the first such tests for high multipoles. They illustrate the effectiveness of the method compared to others, such as Maxwell multipoles (Katz & Weeks 2004; Weeks 2004; Copi et al. 2006, 2007), which run into combinatoric problems at high l (Dennis 2005). We do not use the ILC map, because it is not expected to be reliable for the large l range we consider here. At large l, the *WMAP* team uses the bands $V1$, $V2$, $W1$, $W2$, $W3$ and $W4$ for their final power extraction in the 3- and 5-yr analysis. The $Q1$ and $Q2$ bands were not used in *WMAP* power estimates because they were found to be significantly contaminated by foreground effects.

Our motivation for the study is twofold. First, we are interested in testing whether the anisotropies found in Samal et al. (2008) continue to hold for a larger range of multipoles. Secondly, we wish to test whether additional anomalies in these data may exist. Our tests are not intended to determine whether anomalies come from some physical effect, contamination due to foregrounds or correlations of noise.

In the next section, we briefly review the methodology. In Section 3, we describe how the methodology is applied to the *WMAP* data. In Section 4, we give results for test of statistical isotropy using the power entropy. In Section 5, we test for alignment of different multipoles with the quadrupole axis. In Section 6, we test for statistical isotropy using the alignment entropy. We conclude in Section 7.

2 COVARIANT FRAMES AND STATISTICS ACROSS MULTIPOLES

The CMB temperature fluctuation in each map is conventionally expanded in spherical harmonics

$$T(\hat{n}) = \sum_{lm} a_{lm} Y_{lm}(\hat{n}).$$

The usual power $C_l \sim \sum_m a_{lm} a^*_{lm}$ is rotationally invariant and has no information about anisotropy. The angular orientation of each mode is probed by a unique orthonormal frame $e^\alpha_k\ (l)$ and rotationally invariant eigenvalues $\Lambda_\alpha(l)$. These are obtained by diagonalizing the power tensor A, defined by

$$A_{ij} = < a\,|J_i J_j\,|\,a >,$$
$$= \sum_\alpha e^\alpha_i (\Lambda^\alpha)^2 e^{\alpha *}_j,$$

where J_i is the rotation generator in representation l and index l is suppressed when obvious.

Basic statistics derived from frames are the power entropy $S_{\rm P}$ and the alignment entropy S_X. Entropy is defined as in quantum statistical mechanics. The power–density matrix $\rho_{\rm P} = A/tr(A)$, where tr indicates the trace, is normalized, $tr(\rho_{\rm P}) = 1$, to remove the power. The power entropy $S_{\rm P}$ for each multipole is

$$S_{\rm P} = -tr[\,\rho_{\rm P}\,\log(\,\rho_{\rm P}\,)\,]. \quad (2)$$

Isotropy predicts the maximum entropy

$$S_{\rm P} \rightarrow \log(3) \quad \text{(isotropy)}.$$

Small values of $S_{\rm P}$ indicate anisotropy. Note these measures apply mode-by-mode. The full range is $0 \leq S_{\rm P} \leq \log(3)$, where $S_{\rm P} \rightarrow 0$ for a 'pure state' $\tilde{\Lambda}_1 = 1$ aligned along a single axis.

The alignment entropy S_X is a measure of alignment of frame axes. Let $e^i(l)$ be the 'principal eigenvector' of the power tensor, meaning the one with the largest eigenvalue. Construct a 3×3 matrix X_{ij}:

$$X_{ij} = \sum_{l=l_{\rm min}}^{l_{\rm max}} e^i(l) e^j(l). \quad (3)$$

This tensor probe effectively averages over a range of multipole moments. Normalize by computing $\tilde{X} = X/tr(X)$. The alignment entropy is

$$S_X = -tr(\tilde{X} \log \tilde{X}).$$

3 APPLICATION TO *WMAP* DATA

We use the *WMAP* 3- and 5-years data for our analysis. The *WMAP* team (Hinshaw et al. 2003, 2007) provides foreground-cleaned maps for the *Q, V* and *W* bands. The *V* and *W* bands are used for power spectrum estimation. The *Q* band is not used as it is found to be significantly foreground contaminated. The foreground removal method adopted by *WMAP* is incomplete in the galactic plane. This region is removed by using the $K\,p2$ mask before power spectrum estimation. Applying $K\,p2$ mask also eliminates emissions from the resolved point sources by removing circular area of radii $0\overset{\circ}{.}6$ around the position of each of the sources. There also exist other foreground cleaning procedures that may be interesting to compare (Tegmark, de Oliveira-Costa & Hamilton 2003; Saha, Jain & Souradeep 2006; Eriksen et al. 2007a). Here, we study only the foreground-cleaned maps provided by the *WMAP* team.

3.1 Data preparation

We apply the $K\,p2$ mask to the entire individual foreground-cleaned DA maps. The masked region is filled by a randomly generated CMB signal along with simulated detector noise based on *WMAP*'s noise characteristics appropriate to each of the eight maps.

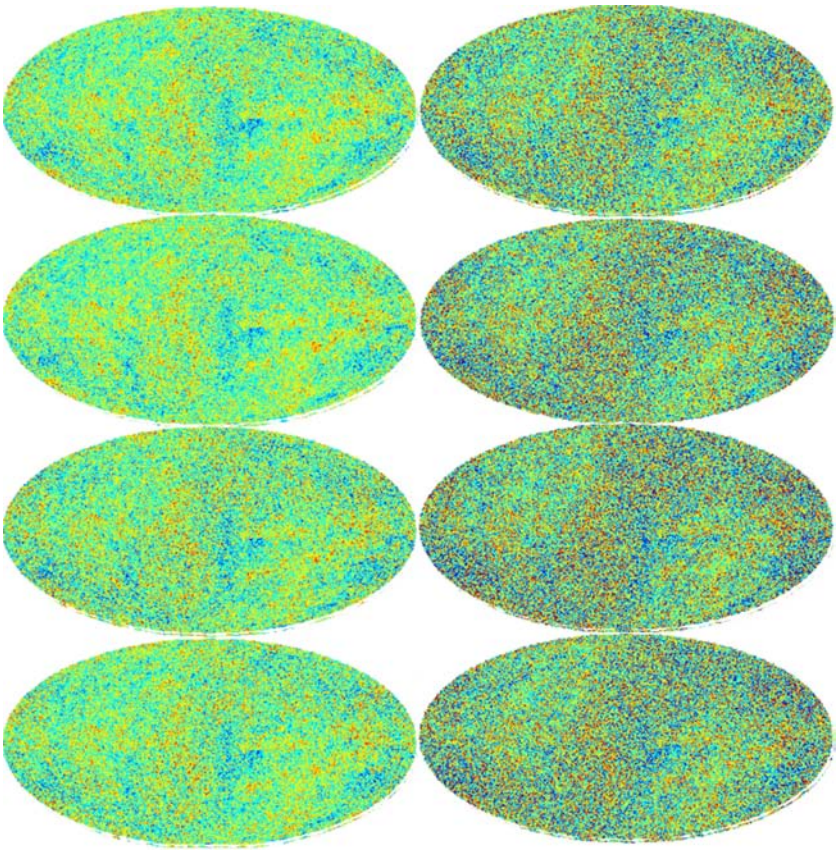

Figure 1. The 3-yr maps after filling the $Kp2$ region with randomly generated CMB signal and detector noise appropriate for each band. From top to bottom the left-hand panel shows $Q1$, $Q2$, $V1$ and $V2$ DA maps, respectively, while the right-hand panel shows $W1$, $W2$, $W3$ and $W4$ DA maps.

Noise maps are generated as follows. Let σ_0 be the noise per observation of the detector under consideration. Let $N_{\rm pix}$ denote the number of pixels in each $N_{\rm side} = 512$ level resolution map, and N_p be the effective number of observations at each pixel. Sample a Gaussian distribution with zero mean and unit variance $N_{\rm pix}$ number of times. Multiply each Gaussian variable by $\sigma_0/\sqrt{N_p}$ to form realistic detector noise maps.

Graphics of the eight maps used in our study are shown in Fig. 1. There is no visible signature of galactic foreground contamination in the maps. Detector noise is evident in the W-band DA maps.

3.2 Null distributions

Statistical baselines were developed from 10 000-run simulations of isotropic random CMB power normalized to the data maps and including detector noise appropriate to each band. We set preliminary levels of statistical significance using P-values of 0.05 or less. P values are defined by the relative frequency for a statistic to occur with P or less. The significance level of collections of P-values is estimated using the binomial distribution of 'pass' and 'fail' outcomes. The probability to encounter k instances of passing defined by probability p in n trials is

$$P_{\rm bin}(k,\ p,\ n) = p^k(1-p)^{(n-k)}n!/(n-k)!k!.$$

The binomial distribution is well known, and we also verified the distribution describes P values from the null simulations. In assessing many P values, we report the cumulative binomial probabilities

$$P_{\rm bin}(k \geq k_*,\ p,\ n) = \sum_{k=k_*}^{n} P_{\rm bin}(k,\ p,\ n).$$

4 POWER ENTROPY

Fig. 2 shows the null distribution of power entropy for the $Q1$ map over the multipole range $2 \leq l \leq 300$. The distribution of all the maps remain the same whether or not detector noise is added to the simulation.

Fig. 3 shows P values obtained from the *WMAP* data for the entire range, $2 \leq l \leq 300$, of multipole values considered. The horizontal dashed line indicates $P = 0.05$. Violation of statistical isotropy is indicated for many multipoles in all the bands. Tables 1 and 2 list the 3-yr (5-yr) multipoles for different bands with P-values potentially inconsistent with isotropy.

Fig. 4 illustrates the entropy distributions leading to these P-values. A contour for the 95 per cent confidence level is shown in grey. The 90 and 50 per cent confidence level contours are also shown as curves. The relatively large spread of the distribution towards the small-l region is kinematic, akin to cosmic variance. The statistically anisotropic multipoles shown by red points are the same as those shown in Table 1.

4.1 Significance: power entropy statistics

We now assess the significance of the numerous small P-values observed for the power entropy.

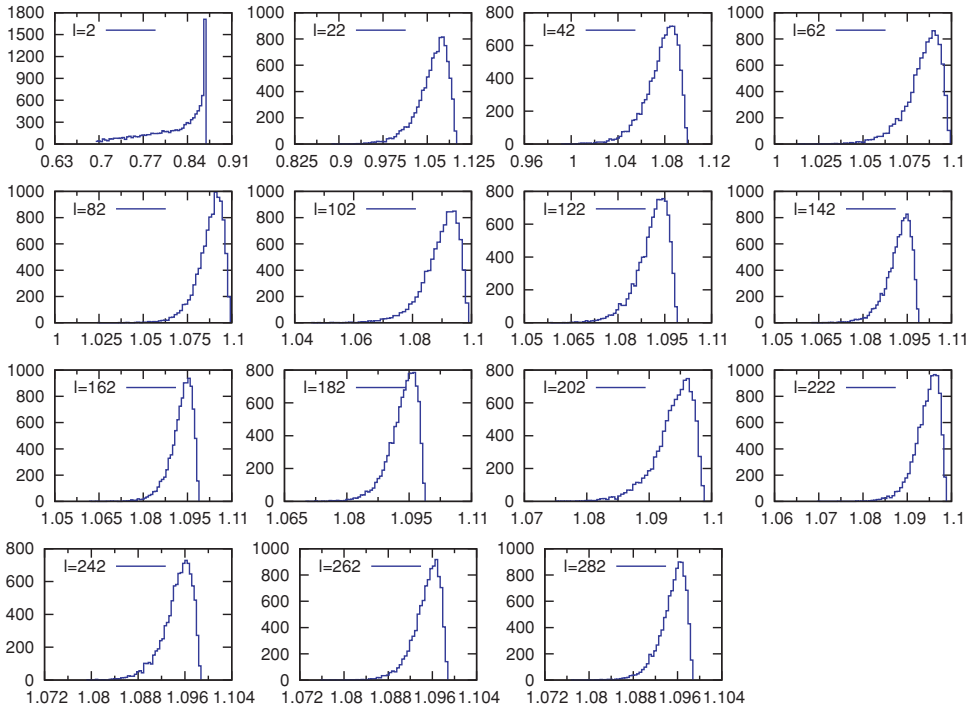

Figure 2. Histograms of the power entropy S_P for multipole range $2 \leq l \leq 300$ at intervals of 20 units using the *WMAP* 3-years data for the $Q1$ map.

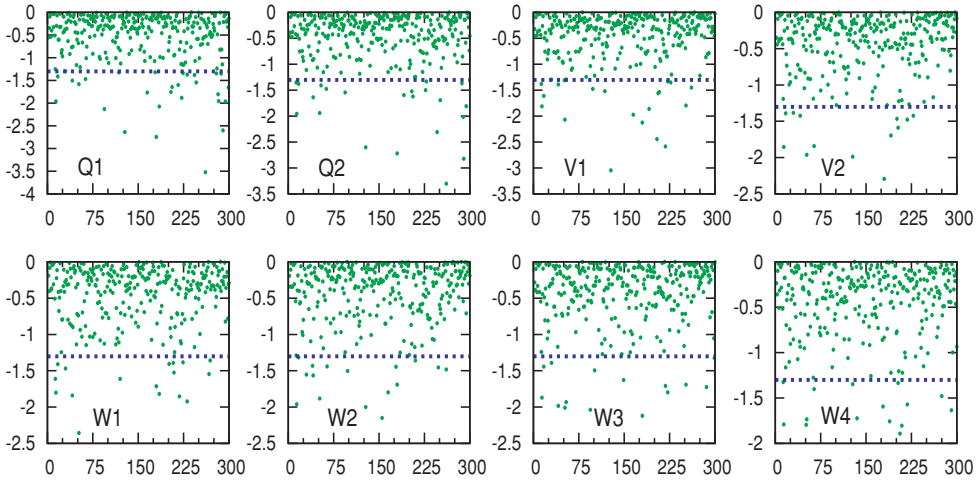

Figure 3. $\log_{10}(P)$ values of the power entropy from the eight *WMAP* bands for the range $2 \leq l \leq 300$ for the *WMAP* 3-years data. The dashed horizontal line shows $P = 0.05$.

Table 1. List of multipoles with $P < 0.05$ for power entropy for the 3-yr *WMAP*-DA maps.

Band	Multipoles
Q1	14, 17, 41, 52, 63, 94, 118, 128, 165, 178, 180, 185, 204, 206, 216, 222, 224, 231, 243, 246, 261, 279, 280, 282, 283, 287, 290, 294, 299
*Q*2	13, 14, 17, 41, 52, 54, 63, 94, 128, 180, 191, 204, 206, 227, 228, 246, 251, 261, 287, 289, 290, 294
*V*1	13, 14, 17, 41, 51, 52, 98, 118, 128, 165, 180, 191, 204, 206, 208, 218, 222, 227, 252, 261
*V*2	14, 17, 30, 41, 52, 64, 128, 180, 191, 201, 203, 218, 228
*W*1	13, 14, 17, 30, 41, 52, 120, 180, 185, 201, 208, 209, 218, 224, 231, 267, 269
*W*2	14, 17, 30, 40, 41, 52, 64, 98, 128, 155, 165, 178, 180, 210, 248, 261
*W*3	14, 17, 30, 41, 52, 54, 94, 101, 149, 180, 218, 222, 252, 286, 299
*W*4	13, 14, 51, 52, 64, 128, 135, 178, 189, 203, 206, 209, 218, 275, 291

Table 2. List of multipoles with $P < 0.05$ for power entropy for the 5-yr *WMAP*-DA maps.

Band	Multipoles
$Q1$	14, 17, 41, 52, 94, 128, 135, 165, 177, 178, 180, 185, 191, 204, 206, 216, 218, 221, 222, 225, 231, 261, 290, 294
$Q2$	13, 14, 17, 41, 52, 54, 94, 128, 165, 170, 180, 191, 204, 206, 228, 246, 251, 261, 290, 294
$V1$	13, 14, 17, 41, 52, 54, 64, 101, 128, 165, 180, 191, 204, 206, 218, 222, 231, 252, 290
$V2$	14, 17, 30, 41, 52, 64, 94, 128, 161, 165, 180, 201, 204, 209, 218, 228
$W1$	13, 14, 17, 30, 41, 52, 64, 120, 128, 139, 180, 185, 201, 204, 210, 218, 224, 228, 231, 269
$W2$	13, 14, 30, 40, 41, 52, 98, 115, 128, 155, 165, 178, 180, 210, 231, 241, 246, 258, 261
$W3$	13, 14, 17, 41, 52, 54, 94, 101, 160, 180, 185, 228, 246, 249
$W4$	13, 14, 41, 52, 64, 94, 128, 135, 170, 180, 189, 201, 204, 206, 210, 241, 242, 252

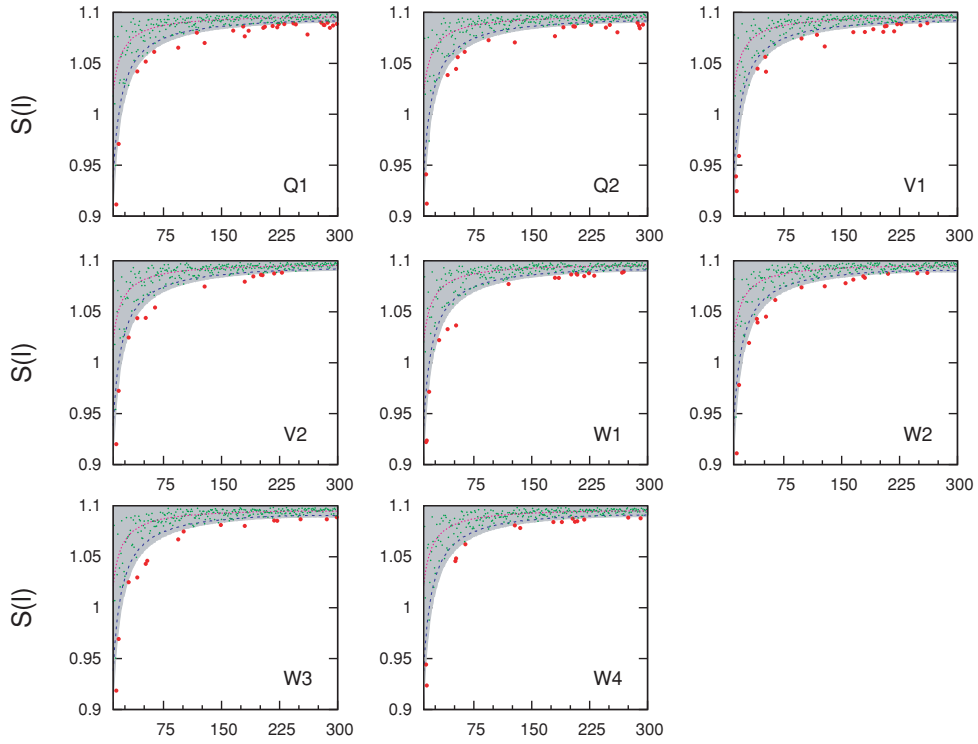

Figure 4. Distribution of the power entropy $S(l)$ showing the 95 per cent confidence level (grey band) for the *WMAP* 3-years data. Red points show multipoles potentially inconsistent with the isotropic prediction.

Tables 1 and 2 show 29 (24), 22 (20), 20 (19), 13 (16), 17 (20), 16 (19), 15 (14) and 15 (18) power entropies with P-value ≤ 0.05 for the 3-yr (5-yr) $Q1$, $Q2$, $V1$, $V2$, $W1$, $W2$, $W3$ and $W4$ maps, respectively. The threshold values (upper bounds of P-values) for these power entropies estimated using the individual maps are given by $\mathcal{P} = 0.048$ (0.047), 0.0467 (0.049), 0.049 (0.049), 0.0412 (0.048), 0.0438 (0.049), 0.0483 (0.047), 0.0472 (0.047) and 0.0473 (0.049). The total number of independent trials for $2 \leq l \leq 300$ is $n = 299$. From the binomial distribution the cumulative probabilities of obtaining $P_{\rm bin}(k \geq k_{\rm data}, P_{\rm data}, 299)$ are shown in Table 3 for the eight maps from $Q1$ to $W4$ for the 3- and 5-yr data.

Clear violation of statistical isotropy is observed for $Q1$ and $Q2$ maps for both the 3- and 5-yr data, which all have $P < 0.05$. We noted in our study that the $Q1$ and $Q2$ P-values are correlated over all l, so we cannot consider them independent. Nevertheless, the cumulative probability of 3×10^{-4} for the $Q1$ band is far below anything expected from an isotropic ensemble.

Table 3. Net significance for obtaining the multipoles with $P \leq 0.05$, listed in Table 1 (3 yr) and Table 2 (5 yr).

Band	$Q1$	$Q2$	$V1$	$V2$
Significance (3 yr)	3×10^{-04}	2.5×10^{-02}	0.10	0.46
Significance (5 yr)	8.2×10^{-03}	0.10	0.15	0.36
Band	$W1$	$W2$	$W3$	$W4$
Significance (3 yr)	0.17	0.37	0.44	0.44
Significance (5 yr)	0.10	0.11	0.54	0.22

If one assumes each probability is independent – which is certainly an idealization – the binomial probability for $Q1$ and $Q2$ for the 3-yr data to have such small probabilities is about 1.6×10^{-2}. Fig. 5 shows the probability of these outcomes over all bands as the 'pass-value' $P_{\rm band} < P_*$ is adjusted for both the 3- and 5-yr data. The small $P_{\rm net}$ values show violation of isotropy. The entire data over all bands show violation of isotropy with a binomial

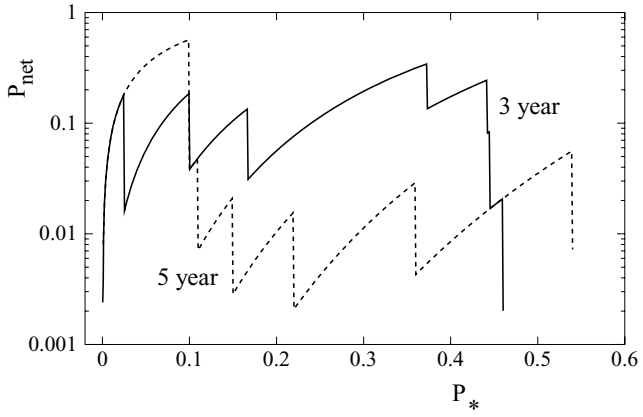

Figure 5. The net probability $P_{\rm net}$ over all the bands selecting power-entropy $P_{\rm band} < P_*$ for the 3- (solid line) and 5-years (dashed line) *WMAP* data.

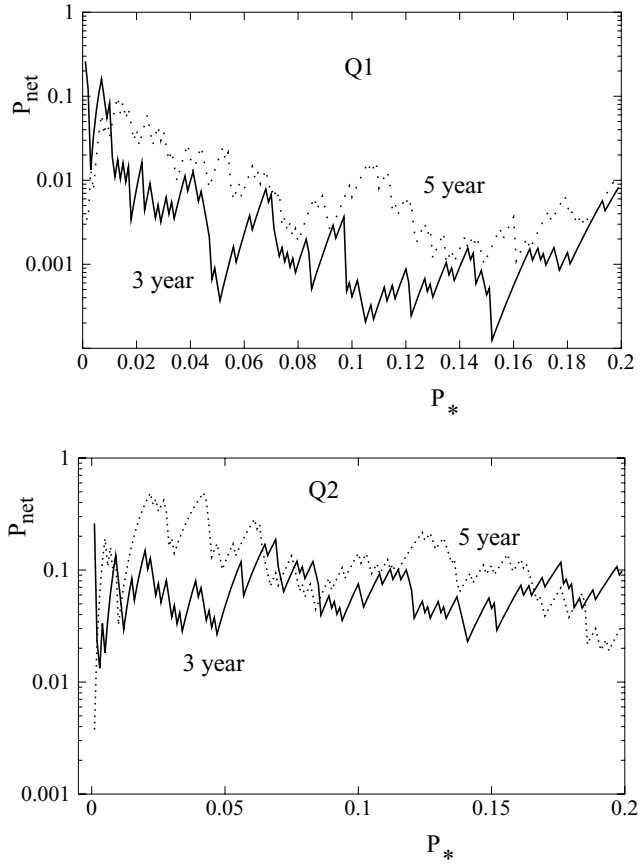

Figure 6. The net cumulative probability $P_{\rm net}$ the DAs $Q1$ and $Q2$ selecting power-entropy $P_{\rm band} < P_*$ for the 3- (solid line) and 5-years (dotted line) *WMAP* data.

probability of 2.0×10^{-3} and 7.2×10^{-3} for the 3- and 5-yr data, respectively.

Because the 5 per cent P-value cut is somewhat arbitrary, Fig. 6 shows the cumulative probability of these outcomes over the $Q1$ and $Q2$ DAs as the 'pass-value' $P_{\rm band} < P_*$ is adjusted for both the 3- and 5-yr data. The small $P_{\rm net}$ values show violation of isotropy. The cumulative probability for the remaining six DAs is shown in Fig. 7. Here, we note that the 3-yr data do not show a significant

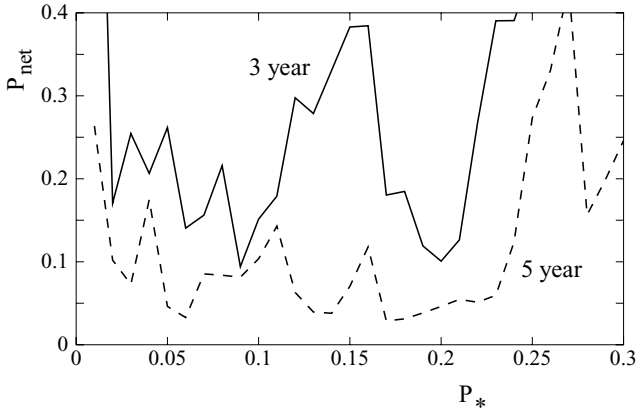

Figure 7. The net cumulative probability $P_{\rm net}$ the DAs $V1$, $V2$, $W1$, $W2$, $W3$ and $W4$ selecting power-entropy $P_{\rm band} < P_*$ for the 3- (solid line) and 5-years (dotted line) *WMAP* data.

violation of isotropy. However, the signal of anisotropy is stronger in the 5-yr data. The trend in this figure suggests that we may expect a much stronger signal of anisotropy in V and W bands as more data are accumulated.

5 ALIGNMENT WITH THE QUADRUPOLE

Many authors (de Oliveira-Costa et al. 2004; Ralston & Jain 2004; Schwarz et al. 2004) have observed a strong alignment between the CMB quadrupole and the octopole. The power of both quadrupole and octopole appears to approximately lie in a plane. The perpendicular to the plane points roughly in the direction of the Virgo supercluster for both these multipoles. It has also been noted that these axes align closely with the CMB dipole, as well as with independent cosmological observations. Statistically significant alignment of several independent axes violates the hypothesis of statistical isotropy. As reported earlier, the *WMAP*-ILC map shows statistically significant signals of alignment with the quadrupole axis in the low l multipole range $l \leq 50$.

In our formalism, one may construct an unbiased measure of alignment between multipoles by comparing the principal eigenvectors of the power tensor. In isotropic data these eigenvectors would point in random directions. The probability for isotropically distributed axes $\hat{n}$ and $\hat{n}'$ to align within θ is given by

$$P(\cos\theta) = (1 - \cos\theta), \tag{4}$$

where $\cos\theta = |\hat{n} \cdot \hat{n}'|$.

5.1 Significance of axial alignments

Tables 4 and 5 list the multipoles with $P(\cos\theta) < 0.05$ for alignment with the quadrupole for 3-yr (5-yr) *WMAP* maps. There are 13 (12), 9 (12), 14 (15), 18 (17), 13 (20), 13 (15), 12 (12) and 11 (18) axes which show alignment with the quadrupole moments for the $Q1$, $Q2$, $V1$, $V2$, $W1$, $W2$, $W3$ and $W4$ maps, respectively, for 3-yr (5-yr) data. The threshold values (upper bound of the P-values) are given by $\mathcal{P} = 0.046$ (0.041), 0.049 (0.047), 0.038 (0.046), 0.048 (0.05), 0.048 (0.049), 0.048 (0.049), 0.044 (0.05) and 0.049 (0.049). The binomial probabilities for each band are, respectively, 0.62 (0.57), 0.96 (0.74), 0.25 (0.39), 0.19 (0.31), 0.68 (0.091), 0.68 (0.50), 0.66 (0.82), 0.87 (0.22) for the 3-yr (5-yr) data. Including the effects of the search over $2 < l \leq 300$, the set of multipole axes examined shows no statistically significant signal of alignment. We

Table 4. List of multipoles with $P < 0.05$ for alignment with the quadrupole for 3-yr *WMAP* data for all the maps for the multipole range $2 \leq l \leq 300$.

$Q1$	$Q2$	$V1$	$V2$	$W1$	$W2$	$W3$	$W4$
2	2	2	2	2	2	2	2
28	28	40	28	28	10	28	40
61	61	50	61	61	28	61	61
63	88	61	63	63	61	62	63
75	101	66	66	81	63	63	88
88	145	75	75	88	75	66	102
105	172	88	81	101	88	75	129
129	176	174	88	133	110	88	133
134	187	198	129	172	129	129	139
140	212	207	144	174	182	133	140
144		226	172	176	197	177	243
145		270	174	182	235	179	272
172		278	182	267	267	265	
182		289	187	279	270		
		293	207				
			243				
			267				
			279				
			293				

Table 5. List of multipoles with $P < 0.05$ for alignment with the quadrupole for 5-yr *WMAP* data over the multipole range $2 \leq l \leq 300$.

$Q1$	$Q2$	$V1$	$V2$	$W1$	$W2$	$W3$	$W4$
2	2	2	2	2	2	2	2
40	40	40	28	28	28	40	3
42	42	42	40	40	40	50	40
61	61	50	50	61	50	61	42
75	88	61	61	63	61	75	61
81	101	75	63	75	63	88	63
88	134	88	66	81	75	133	88
101	172	101	75	88	88	226	101
105	176	129	88	101	133	236	129
129	187	140	101	129	179	243	133
134	195	174	129	133	182	265	139
182	238	182	172	172	207	270	172
		207	174	174	267		176
		279	182	178	270		177
		300	187	182	171		197
			279	187			243
			293	234			266
				267			272
				278			
				279			

point out, however, that the overall probabilities have a tendency to decrease as we go from 3- to 5-yr data.

There are several differences between the data set used in the previous study and the one used for the present analysis. The previous study used the ILC map, which is ideal for low l multipoles. This is because the ILC map has lower foregrounds and the entire map can be used. The template cleaned maps are best suited for large l multipoles and require a mask to remove the contamination due to galactic and point source emissions. In addition, the high l data also contain very large detector noise contamination, tending to decrease signal-to-noise ratio.

6 ALIGNMENT ENTROPY

We next consider the alignment entropy S_X over the entire range of multipoles $2 \leq l \leq 300$, and a few selected subsets, $150 \leq l \leq 300$ and $250 \leq l \leq 300$. Figs 8 and 9 show null distributions of S_X for the range $150 \leq l \leq 300$ and $2 \leq l \leq 300$. These distributions are generated by simulated CMB data along with detector noise, appropriate for a particular map. The distribution of S_X for the two cases is nearly identical. These distributions are similar to the power entropy distributions, consisting of sharp suppression of small S_X below a peak near the maximum. The S_X distributions for small l show a long tail. Figs 8 and 9 also show the value of S_X obtained from the data for all cases except the maps $Q1$ and $Q2$. For these two maps the value of S_X lies outside the range shown in the plots.

The values of S_X for all the maps for the 3-yr *WMAP* data are shown in Table 6. The probabilities of obtaining these values from a random isotropic sample are also shown. These are computed by using 10 000 randomly generated samples of isotropic CMB maps including detector noise. The statistics are interesting. In all three sets the Q band shows a very significant signal of violation of statistical isotropy. The probability that the entropy obtained for $Q1$ map arises by a random fluctuation is less than 0.01 per cent for all three range of multipoles considered. The map $Q2$ also shows very low probability values.

The preferred axes of alignment over the different ranges of multipoles are given in Table 7. We find that the axes do not point towards any familiar direction. The axes do not point towards Virgo and hence are not aligned with the quadrupole. They tend to lie within about 30° from the galactic plane at the galactic longitude ranging between 90° and 100°. We next determine the mean axis in a simulated $Q1$ map in the range $2 \leq l \leq 300$. Foregrounds are added to this map by using the publicly available Planck Sky Model (PSM)[1] as reference templates. We add foregrounds at the level of 1, 2, . . . , 10 per cent of the total contamination and determine the mean vector for each map. The mean vector is determined after applying the $K\,p2$ mask and filling the masked region with randomly generated data, exactly as done for the real data set. As expected at low foreground level the mean axis fluctuates considerably for different realizations of the randomly generated maps. However, at foreground levels of 5 per cent or higher, the mean axes stabilize. They also do not show much change with the increase in the level of contamination. The axes are found to lie between $b = 25°$–$28°$, $l = 150°$–$167°$ for foreground levels of 5 per cent or higher of their total values.

We compare the axes obtained using randomly generated maps with the axes given in Table 7. We find that the galactic latitude matches well with that obtained from the real data. However, the longitude is off by almost 60°–70°. Hence, it is not possible to assign the alignment we find to contamination due to known foregrounds. The randomly generated axes depend to some extent on the range of multipoles studied. For the multipole range $250 \leq l \leq 300$, the mean axis is found to be roughly $b = 6°$, $l = 125°$. This is a little closer to corresponding value in this range in Table 7. We note, however, that dependence of the axis on the choice of multipole range is much stronger in the randomly generated data in comparison to that found in Table 7. This again shows that we cannot attribute the anisotropy in Q band to known foregrounds. It is possible that the anisotropy

[1] We acknowledge the use of version 1.1 of the Planck reference sky model, prepared by the members of Working Group 2 and available at http://www.planck.fr/heading79.html.

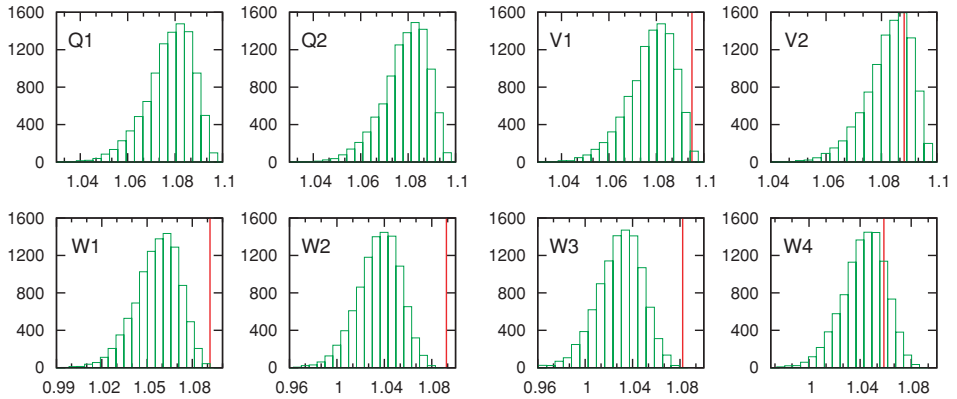

Figure 8. The distribution of the alignment entropy for the statistically isotropic CMB plus appropriate detector noise maps for the range $150 \leq l \leq 300$ for the *WMAP* 3-years data. The alignment entropy measures for different maps are also shown.

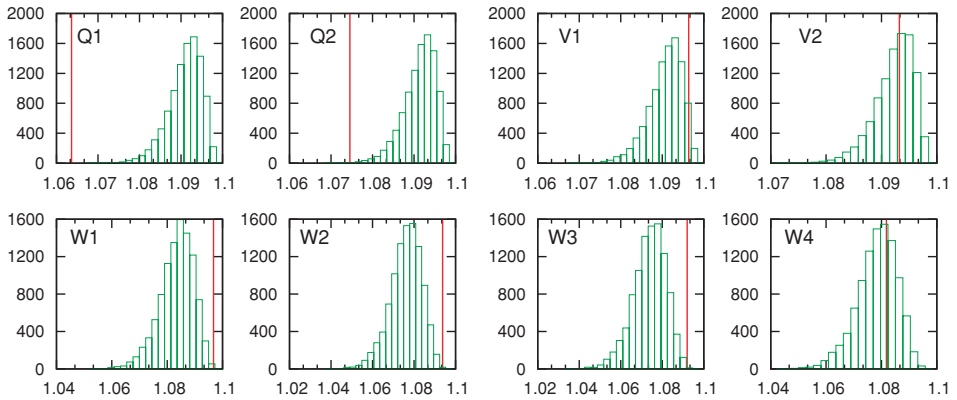

Figure 9. The distribution of the alignment entropy for the statistically isotropic CMB plus appropriate detector noise maps for the range $2 \leq l \leq 300$ for the *WMAP* 3-years data. The alignment entropy measures for different maps are also shown.

Table 6. Alignment entropy S_X and corresponding P-values (in per cent) for *WMAP* 3-yr maps over the three multipole ranges, $2 \leq l \leq 300$, $150 \leq l \leq 300$ and $250 \leq l \leq 300$.

$Q1$	$Q2$	$V1$	$V2$	$W1$	$W2$	$W3$	$W4$	
$S_X(150, 300)$	0.98522	1.02024	1.09499	1.08822	1.09174	1.09234	1.08222	1.05858
P(per cent)	<0.01	<0.01	99.25	72.08	99.98	>99.99	>99.99	82.10
$S_X(250, 300)$	0.79763	0.92503	1.077021	1.08415	1.055178	1.07635	0.98258	1.019228
P(per cent)	<0.01	0.36	94.72	94.89	97.36	99.9	86.56	92.03
$S_X(2, 300)$	1.0636	1.0745	1.0964	1.0932	1.0967	1.0937	1.0920	1.0818
P(per cent)	<0.01	0.15	95.86	53.94	99.94	99.74	99.91	65.52

Table 7. The galactic latitude (b) and longitude (l) for the principal axis for the specified range of multipole moments for *WMAP* 3-yr $Q1$ and $Q2$ bands.

$Q1$ band	b (°)	l (°)
$150 \leq l \leq 300$	27.8	97.8
$250 \leq l \leq 300$	30.2	101.5
$2 \leq l \leq 300$	24.7	92.9
$Q2$ band	b (°)	l (°)
$150 \leq l \leq 300$	26.3	94.6
$250 \leq l \leq 300$	28.1	99.2
$2 \leq l \leq 300$	22.2	89.7

arises due to an unknown foreground source or from a combination of foregrounds and other effects.

The V and W bands reveal an unexpected number of cases with very large alignment entropy, corresponding to unusually perfect isotropy. We find several cases in the W band where the alignment entropy is so large that the probability to obtain this from a random sample exceeds 99.99 per cent.

Similar results are seen for the 5-yr *WMAP* data. In Table 8, we show the alignment entropy S_X and probabilities P for all the maps in the three multipole ranges considered. We again find that the Q band shows a very striking signal of anisotropy. The W band, on the other hand, again shows an improbably high level of isotropy. The V band does not appear statistically unusual. Table 9 shows the axes

Table 8. The alignment entropy and the corresponding P-values (in per cent) for the *WMAP* 5-yr DA maps. The results for all the three multipole ranges considered in this paper are shown.

	$Q1$	$Q2$	$V1$	$V2$	$W1$	$W2$	$W3$	$W4$
$S_X(150, 300)$	1.00795	1.02283	1.09116	1.08587	1.08633	1.09417	1.09522	1.08451
P(per cent)	<0.01	<0.01	75.7	31.5	87.8	>99.99	>99.99	94.3
$S_X(250, 300)$	0.85946	0.89287	1.08185	1.08579	1.08321	1.08854	1.05246	1.07737
P(per cent)	<0.01	<0.01	86.0	85.9	98.8	99.9	96.9	99.4
$S_X(2, 300)$	1.07100	1.07602	1.09462	1.09283	1.09362	1.09259	1.09694	1.08896
P(per cent)	<0.01	<0.01	60.1	28.6	83.3	93.6	99.98	61.6

Table 9. The galactic latitude (b) and longitude (l) for the principal axis for the specified range of multipole moments for *WMAP* 5-yr $Q1$ and $Q2$ bands.

$Q1$ band	b (°)	l (°)
$150 \leq l \leq 300$	24.6	98.2
$250 \leq l \leq 300$	27.3	103.2
$2 \leq l \leq 300$	20.2	93.1
$Q2$ band	b (°)	l (°)
$150 \leq l \leq 300$	29.6	94.7
$250 \leq l \leq 300$	32.2	97.3
$2 \leq l \leq 300$	24.0	88.9

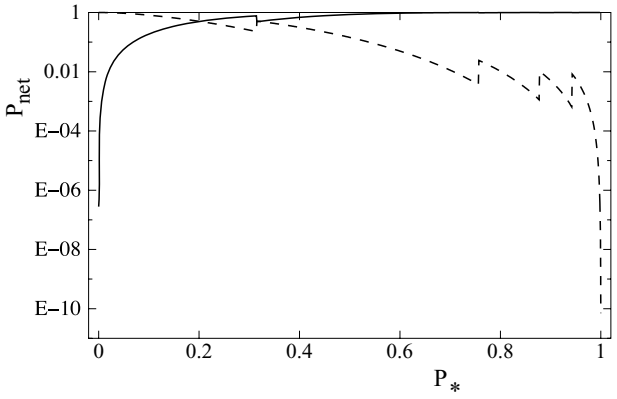

Figure 10. The net probability $P_{\rm net}$ across bands to find excessive anisotropy (solid line) and isotropy (dashed line) with the alignment entropy for the *WMAP* 5-years data. Multipole range $150 \leq l \leq 300$.

of alignment for the Q band. The axes are found to be consistent with that found in the 3-yr data.

Fig. 10 shows the net probability across bands for $P < P_*$ or 'excessive anisotropy' as well as $P > P_*$, or 'excessive isotopy' for the 5-yr data.

6.1 Foreground contamination in Q band

One might naturally assume the anisotropy found in the Q band would be due to foreground contamination. The principal vectors for all the multipole ranges considered here cannot be consistently attributed to known foregrounds. Let us nevertheless assume that foregrounds give a significant contribution to the Q-band anisotropy, and seek the mean foreground power required to explain the observations. We restrict this study to the multipole range $150 \leq l \leq 300$.

To estimate residual foreground contamination in the maps we use PSM as reference templates. We first generate a composite foreground map corresponding to each map using synchrotron, dust and free–free maps obtained by PSM. We apply the $Kp2$ mask to the entire composite foreground maps also in order to avoid strong contamination arising from the galactic region. Finally, we add a small fraction of the composite foreground contamination arising from these masked templates to a randomly generated CMB map, plus simulated detector noise appropriate to each maps. We finally compute the alignment entropy for each band.

The residual foreground contamination in regions not affected by the $Kp2$ mask was estimated from the fraction of the composite masked foreground template added to randomly generated CMB maps. We obtain the full-sky estimates of the foreground contamination using the Monte Carlo Apodized Spherical Transform Estimator (MASTER) method (Hivon et al. 2002) which employs inversion of the mode–mode coupling matrix to convert the partial-sky power spectrum to full-sky estimates.

In Fig. 11, we show the alignment entropy as a function of the average value of the full-sky estimates of the residual foreground

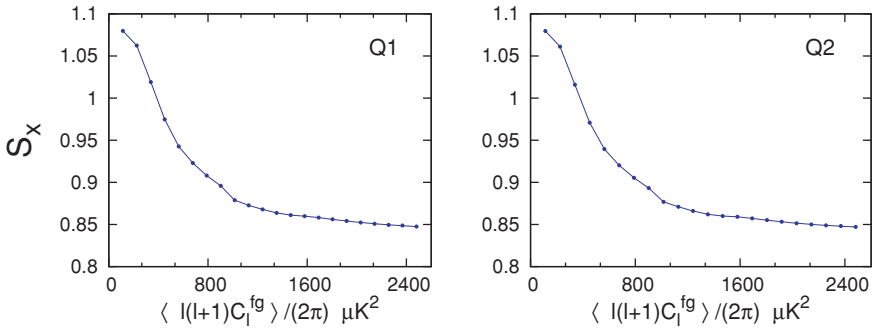

Figure 11. The alignment entropy, S_X, for the bands $Q1$ and $Q2$ for the multipole range $150 \leq l \leq 300$ as a function of the average foreground power (see text).

Table 10. The average foreground residual power, $< l(l+1)C_l^{\rm fg} >/(2\pi)$, for the *WMAP* 3-yr and 5-yr $Q1$ and $Q2$ maps, which show significant signals of anisotropy with $P \leq 0.01$ per cent for the multipole range $150 \leq l \leq 300$. The foreground power has been averaged over this range of multipoles, as explained in text.

Maps	$Q1$	$Q2$
Average Foreground Power (μ K^2)	420.72 (3 yr) 417.33 (5 yr)	330.48 (3 yr) 375.73 (5 yr)

contamination for each band for the multipole range $150 \leq l \leq 300$. We estimate the average foreground power for the range of multipole moment $l_{\rm min} \leq l \leq l_{\rm max}$ as

$$\left\langle l(l+1)C_l^{\rm fg} \right\rangle = \frac{1}{(l_{\rm max} - l_{\rm min} + 1)} \sum_{l=l_{\rm min}}^{l_{\rm max}} l(l+1)C_l^{\rm fg}, \quad (5)$$

where $C_l^{\rm fg}$ is the foreground power spectrum at l. For a given value of the entropy obtained from the data, this figure gives the average level of residual foreground contamination in the range of multipoles under consideration. The $Q1$ and $Q2$ maps indicate a strong level of foreground contamination for the multipole range $150 \leq l \leq 300$. Table 10 shows the estimated residual foreground contamination quantitatively.

6.2 Isotropy in *V* and *W* bands

The very striking result seen in Table 6 is the unusually high P-values for many of the multipoles in the V and W bands for the 3-years *WMAP* data. This anomaly is also supported by the *WMAP* 5-yr data for the W band. This is very unexpected and shows a statistically unusual high level of isotropy. We are unable to identify the cause of this anomaly. One possibility is the neglect of noise correlations in our analysis. The anomaly is ameliorated if we artificially lower the detector noise level in the simulated random maps. The σ_0 values used for generating the noise maps for the bands $Q1$, $Q2$, $V1$, $V2$, $W1$, $W2$, $W3$ and $W4$ are 2.245, 2.135, 3.304, 2.946, 5.883, 6.532, 6.885 and 6.744, respectively. Fig. 12 shows the generated noise maps for the bands $Q1$ and $W2$. The $W2$ map over the range $150 \leq l \leq 300$ shows a P-value of 100 per cent. To explore this, we studied how the P-value changes using a smaller value of σ_0. Reducing σ_0 by two units to 4.532, the P-value decreases to a more reasonable value of 92 per cent. However, we find such a large change in the value of σ_0 unacceptable. The problem of statistically unlikely isotropy is not solved in the present paper.

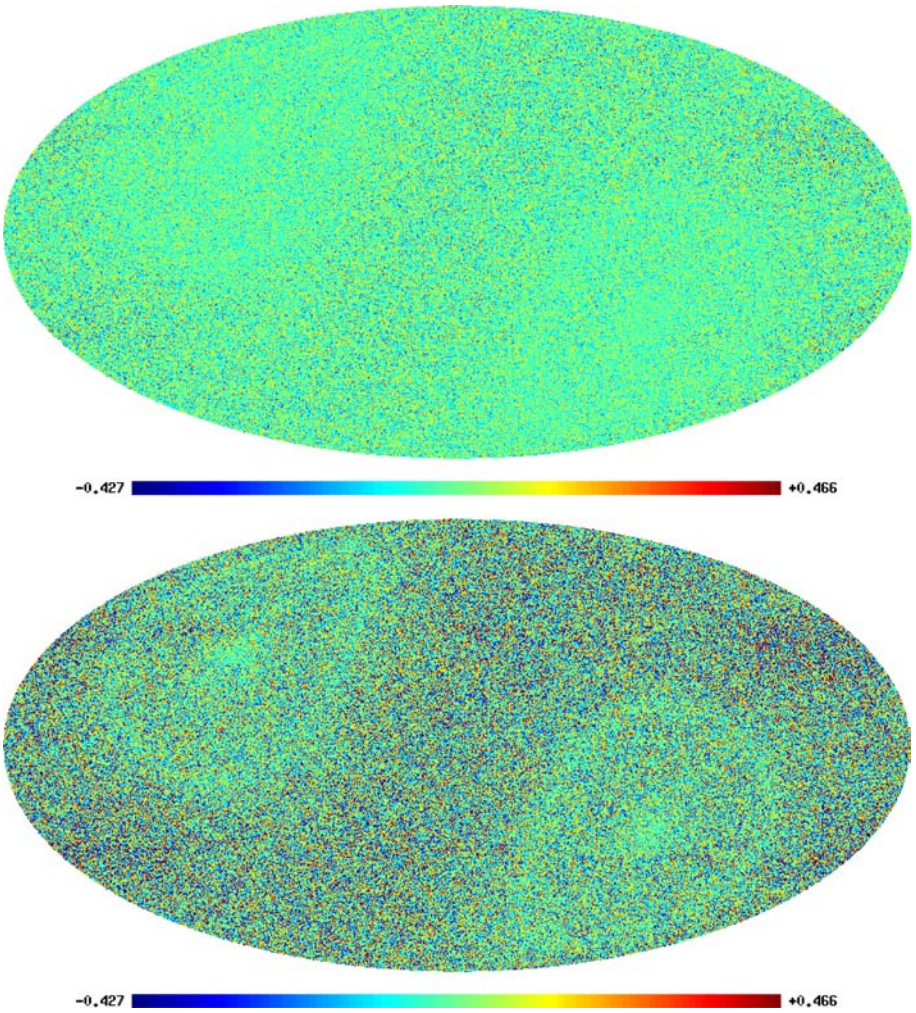

Figure 12. The generated noise maps for $Q1$ (upper) and $W4$ (lower) bands.

7 CONCLUSIONS

The possible violation of isotropy in CMB has been a subject of intense research after the publication of *WMAP* data. The possible alignment of axes corresponding to several diverse data sets in the direction of the Virgo cluster makes this extremely interesting. Despite several proposals the origin of this effect is so far unknown.

We have developed a general method to test for statistical isotropy in the CMB data. The method assigns three orthogonal eigenvectors and the corresponding eigenvalues for each l multipole. The dispersion in the eigenvalues is quantified by defining the concept of power entropy and provides a measure of the violation of statistical isotropy. The principal eigenvector, i.e. the eigenvector corresponding to maximum eigenvalue, can also be compared across different multipoles. This yields another measure of violation of isotropy. We also define the concept of alignment entropy which tests for dispersion in the principal eigenvectors across a range of l values. We apply these techniques to the foreground-cleaned DA maps provided by the *WMAP* team for their 3- and 5-yr data.

We find that some of the DA maps, particularly those corresponding to Q band, show signal of significant violation of statistical isotropy. We are unable to attribute this violation to known foreground contamination. Assuming that the signal arises dominantly due to foregrounds, we obtain an estimate of the residual foreground contamination in these maps. We also find a significant signal of anisotropy if we combine the results obtained from all the DAs. The V and W bands do not by themselves yield a significant signal of anisotropy. However, the violation of isotropy in these DAs is much stronger in the 5-yr data in comparison to the 3-yr data. This suggests that the signal of anisotropy in these data sets may be masked by the presence of large detector noise and may become much more significant as we accumulate more data.

We do not find a signal of significant alignment with the quadrupole in the present data. In an earlier paper (Samal et al. 2008), we did find a significant signal in the ILC map in the low multipole range. In this range of multipoles, the ILC map is most reliable. This leads us to conclude that alignment with the quadrupole may be present only at low multipoles. The presence of residual foregrounds and detector noise in individual DA maps, however, may hide a signal of alignment. In our studies using alignment entropy, we find a highly significant signal of anisotropy for the Q band. This is consistent with the results we found using power entropy. A conservative interpretation is that the Q-band anisotropy arises due to residual foregrounds. However, we are unable to attribute the alignment in the Q to known foregrounds. The principal axes, for all the multipole ranges considered, are consistent with one another and do not agree well with those found by using simulated data with PSM foreground templates. Our results indicate the existence of some unknown foreground contamination or some other effect.

In the W band, we find an improbable level of isotropy in the data. This is quite unexpected. We considered whether this might be due to incorrect assumptions in our random simulations. Yet, the assumptions we make are standard. Excess isotropy appears to be a serious problem. This has implications beyond the issues addressed here. It would be interesting to test the common assumption that detector noise is inherently uncorrelated. The question is important because incorrect modelling of detector noise may also lead to bias in the estimation of CMB power and the cosmological parameters.

ACKNOWLEDGMENTS

We acknowledge the use of Legacy Archive for Microwave Background Data Analysis. Some of the results of this work are derived using the publicly available HEALPIX package (Górski et al. 2005). PKS acknowledges CSIR, India for financial support under the research grant CSIR-SRF-9/92(340)/2004-EMR-I. JPR is supported in part under DOE Grant Number DE-FG02-04ER14308. A portion of the research described in this paper was carried out at the Jet Propulsion Laboratory, California Institute of Technology, under a contract with the National Aeronautics and Space Administration.

REFERENCES

Abramo L. R., Sodre L. Jr., Wuensche C. A., 2006, Phys. Rev. D, 74, 083515
Armendariz-Picon C., 2004, JCAP, 0407, 007
Armendariz-Picon C., 2006, JCAP, 0603, 002
Battye R. A., Moss A., 2006, Phys. Rev. D, 74, 04130
Berera A., Buniy R. V., Kephart T. W., 2004, JCAP, 0410, 016
Bernui A., 2008, Phys. Rev. D, 78, 063531
Bernui A., Villela T., Wuensche C. A., Leonardi R., Ferreira I., 2006, A&A, 454, 409
Bernui A., Mota B., Reboucas M. J., Tavakol R., 2007, A&A, 464, 479
Bielewicz P., Górski K. M., Banday A. J., 2004, MNRAS, 355, 1283
Bielewicz P., Eriksen H. K., Banday A. J., Górski K. M., Lilje P. B., 2005, ApJ, 635, 750
Bietenholz M. F., Kronberg P. P., 1984, ApJ, 287, L1
Birch P., 1982, Nat., 298, 451
Boehmer C. G., Mota D. F., 2008, Phys. Lett. B, 663, 168
Buniy R. V., Berera A., Kephart T. W., 2006, Phys. Rev. D, 73, 063529
Campanelli L., Cea P., Tedesco L., 2007, Phys. Rev. D, 76, 063007
Cline J. M., Crotty P., Lesgourgues J., 2003, JCAP, 0309, 010
Contaldi C. R., Peloso M., Kofman L., Linde A., 2003, JCAP, 0307, 002
Copi C. J., Huterer D., Schwarz D. J., Starkman G. D., 2006, MNRAS, 367, 79
Copi C. J., Huterer D., Schwarz D. J., Starkman G. D., 2007, Phys. Rev. D, 75, 023507
de Oliveira-Costa A., Tegmark M., 2006, Phys. Rev. D, 74, 023005
de Oliveira-Costa A., Tegmark M., Zaldarriaga M., Hamilton A., 2004, Phys. Rev. D, 69, 063516
Dennis M. R., 2005, J. Phys. A, 38, 1653, preprint (math-ph/0410004)
Donoghue E. P., Donoghue J. F., 2005, Phys. Rev. D, 71, 043002
Donoghue J. F., Dutta K., Ross A., 2007, preprint (astro-ph/0703455)
Efstathiou G., 2003, MNRAS, 346, L26
Eriksen H. K., Hansen F. K., Banday A. J., Górski K. M., Lilje P. B., 2004, ApJ, 605, 14
Eriksen H. K. et al., 2007a, ApJ, 656, 641
Eriksen H. K., Banday A. J., Górski K. M., Hansen F. K., Lilje P. B., 2007b, ApJ, 660, L81
Freeman P. E., Genovese C. R., Miller C. J., Nichol R. C., Wasserman L., 2006, ApJ, 638, 1
Gaztanaga E., Wagg J., Multamaki T., Montana A., Hughes D. H., 2003, MNRAS, 346, 47
Gordon C., Hu W., Huterer D., Crawford T., 2005, Phys. Rev. D, 72, 103002
Górski K. M., Hivon E., Banday A. J., Wandelt B. D., Hansen F. K., Reinecke M., Bartelmann M., 2005, ApJ, 622, 759
Gumrukcuoglu A. E., Contaldi C. R., Peloso M., 2007, JCAP, 0711, 005
Hajian A., Souradeep T., 2006, Phys. Rev. D, 74, 123521
Hajian A., Souradeep T., Cornish N. J., 2004, ApJ, 618, L63
Hansen F. K., Banday A. J., Górski K. M., 2004, MNRAS, 354, 641
Helling R. C., Schupp P., Tesileanu T., 2007, Phys. Rev. D, 74, 063004
Hinshaw G. et al., 2003, ApJS, 148, 63
Hinshaw G. et al., 2007, ApJS, 170, 288
Hivon E., Górski K. M., Netterfield C. B., Crill B. P., Prunet S., Hansen F., 2002, ApJ, 567, 2
Hunt P., Sarkar S., 2004, Phys. Rev. D, 70, 10 3518
Hutsemékers D., 1998, A&A, 332, 41

Hutsemékers D., Lamy H., 2001, A&A, 367, 381
Hutsemékers D., Payez A., Cabanac R., Lamy H., Sluse D., Borguet B., Cudell J.-R., 2008, in Bastien P., Manset N., eds, Astronomical Polarimetry 2008. Science from Small to Large Telescopes. Astron. Soc. Pac., San Francisco, in press (arXiv:0809.3088)
Inoue K. T., Silk J., 2006, ApJ, 648, 23
Jain P., Ralston J. P., 1999, Mod. Phys. Lett. A, 14, 417
Jain P., Sarala S., 2006, J. Astrophys. Astron., 27, 443
Jain P., Panda S., Sarala S., 2002, Phys. Rev. D, 66, 085007
Jain P., Narain G., Sarala S., 2004, MNRAS, 347, 394
Land K., Magueijo J., 2005, Phys. Rev. D, 72, 101302
Land K., Magueijo J., 2006, MNRAS, 367, 1714
Land K., Magueijo J., 2007, MNRAS, 378, 153
Lew B., 2008, JCAP, 09, 023
Liu H., Li T.-P., 2008, preprint (arXiv:0806.4493)
Kahniashvili T., Lavrelashvili G., Ratra B., 2008, Phys. Rev. D, 78, 063012
Kanno S., Kimura M., Soda J., Yokoyama S., 2008, JCAP, 0808, 034
Katz G., Weeks J., 2004, Phys. Rev. D, 70, 063527
Kendall D. G., Young A. G., 1984, MNRAS, 207, 637
Kesden M. H., Kamionkowski M., Cooray A., 2003, Phys. Rev. Lett., 91, 221302 (astro-ph/0306597)
Koivisto T., Mota D. F., 2006, Phys. Rev. D, 73, 083502
Koivisto T., Mota D. F., 2008, ApJ, 679, 1
Magueijo J., Sorkin R. D., 2007, MNRAS, 377, L39
Moffat J. W., 2005, JCAP, 0510, 012
Naselsky P. D., Verkhodanov O. V., Nielsen M. T. B., 2008, Astrophysical Bulletin, 63, 216
Payez A., Cudell J. R., Hutsemékers D., 2008, preprint (arXiv:0805.3946)
Pereira S., Pitrou C., Uzan J.-P., 2007, JCAP, 0709, 006
Prunet S., Uzan J.-P., Bernardeau F., Brunier T., 2005, Phys. Rev. D, 71, 083508
Rakic A., Rasanen S., Schwarz D. J., 2006, MNRAS, 369, L27
Ralston J. P., Jain P., 2004, Int. J. Mod. Phys. D, 13, 1857
Rodrigues D. C., 2008, Phys. Rev. D, 77, 023534
Saha R., Jain P., Souradeep T., 2006, ApJ, 645, L89
Samal P. K., Saha R., Jain P., Ralston J. P., 2008, MNRAS, 385, 1718
Schwarz D. J., Starkman G. D., Huterer D., Copi C. J., 2004, Phys. Rev. Lett., 93, 221301
Slosar A., Seljak U., 2004, Phys. Rev. D, 70, 083002
Tegmark M., de Oliveira-Costa A., Hamilton A., 2003, Phys. Rev. D, 68, 123523
Vale C., 2005, preprint (astro-ph/0509039)
Weeks J. R., 2004, preprint (astro-ph/0412231)
Wiaux Y., Vielva P., Martinez-Gonzalez E., Vandergheynst P., 2006, Phys. Rev. Lett., 96, 151303
Yokoyama S., Soda J., 2008, JCAP, 0808, 005

This paper has been typeset from a TEX/LATEX file prepared by the author.